IEEE Open Journal of
Antennas and Propagation

Received 17 October 2021; revised 12 November 2021; accepted 24 November 2021. Date of publication 29 November 2021;
date of current version 8 December 2021.

Digital Object Identifier 10.1109/OJAP.2021.3131242

A Wideband L-Probe Fed Conformal Antenna Array Using Metasurface

S. HUANG[1], C. F. ZHOU[2] (Member, IEEE), J. X. SUN[2], S. S. YUAN[2], H. LI[2], X. M. DING[3], Q. WU[3] (Senior Member, IEEE), AND X. B. TANG[1]

[1]China Academic Electronic and Information Technology, Beijing 100041, China

[2]School of Information and Communication Engineering, Dalian University of Technology, Dalian 116024, China

[3]Advanced Microscopy and Instrumentation Research Center, Harbin Institute of Technology, Harbin 150080, China

CORRESPONDING AUTHORS: C. F. ZHOU and X. M. DING (e-mail: cfzhou@dlut.edu.cn; xuminding@hit.edu.cn)

This work was supported in part by the National Natural Science Foundation of China under Grant 62001080,
and in part by the Natural Science Foundation of Heilongjiang Province under Grant YQ2021F004.

ABSTRACT A wideband conformal metasurface (MTS) antenna array with high gain is designed in this paper. The cooperation of the MTS and L-probe feeding of the antenna element realizes a wide bandwidth of 28.1%, which exhibits only one resonant mode. Then, the planar and conformal arrays consisting of 4×8 MTS antenna elements are investigated. The planar and conformal antenna arrays are fabricated and measured. The measured result shows that when the bending angle $\theta \leq 10°$, unidirectional radiation and high gain can be maintained. The planar antenna array shows a measured impedance bandwidth (IMBW) of 2.81-3.76 GHz (0.95 GHz, 29.7%), with a peak gain of 22.2 dBi, and the conformal antenna array for the bending angle of 10° exhibits an IMBW of 2.8-3.63 GHz (0.82 GHz, 25.6%), with a peak gain of 20.2 dBi.

INDEX TERMS Metasurface, wideband, antenna array, conformal.

I. INTRODUCTION

METASURFACE (MTS) has demonstrated various unusual properties, which can lead to many abnormal phenomena and novel devices [1]–[3]. MTSs are composed of periodic 2-D sub-wavelength elements, owning the advantages of low profile, easy fabrication, and low insertion loss [4], [5]. By arranging the elements in different shapes, the MTS behaves differently, such as anomalous refraction/reflection [6], polarization rotation [7], [8], and radar cross section (RCS) reduction [9], [10]. MTS has also been proved to be a good candidate for increasing the bandwidth of low-profile antennas [11]–[16]. Recently, TM leaky wave mode and TE surface mode were excited to achieve an impedance bandwidth (IMBW) of 34.5% [11]. By feeding the mushroom metamaterial with a slot antenna [12], TM10 and anti-phased TM20 modes were generated simultaneously to acquire an IMBW of 28%. The MTS was also used to improve the axial ratio bandwidth of a cross slot antenna with gain enhancement [13]. To expand the IMBW, three modes including the leaky wave mode, surface wave mode, and dipole mode were excited to achieve an IMBW of 36% with dual polarizations [14].

Recently, various platforms, such as aircrafts, unmanned aerial vehicles (UAVs), and automobiles, have raised more and more demands on antennas [17]–[19]. To satisfy the aerodynamic requirements, conformal antennas are required to mount the shapes of non-planar platforms. Considering the available fabrication and low-cost manufacturing techniques, ultrathin substrates with a thickness of 0.5 mm is adopted for easy bending the antenna, which can be integrated with the non-planar surface. Thus, the discontinuity and air drag of the structure are mitigated while keeping the aerodynamics and aesthetics of the mounting platforms. Many conformal antennas have been proposed [20]–[22], but most of them focus on the antenna element design, which are not suitable for the array design. Due to the

unique characteristic of the MTS, the investigation of conformal MTS has been conducted [23]–[30]. Many works just focus on the MTS design [23]–[25]. For example, a conformal MTS using the phase cancellation technique based on multi elements, was proposed to achieve wideband RCS reduction [23]. An ultrathin reflective polarization converter was engineered to convert the co-polarization to cross-polarization with high efficiency [24]. Many conformal metasurfaces are combined with a feeding antenna to achieve a high gain or polarization conversion [26]–[30]. The rounded MTS was implemented for linear-to-circular polarization conversion [26]. A monopole antenna was placed at the center of the rounded MTS as the feed source. Thus, omnidirectional circular polarization radiation was achieved. To enhance the antenna gain, a conformal compensated-phase partially reflective surface (PRS) was combined with a patch antenna [27]. An ultrathin dual-layer Huygens MTS was constructed to develop a conformal transmitarray with high efficiency [28]. However, these works are not suitable for the antenna array application.

As MTS can enhance the antenna performances with a low profile, a conformal MTS based antenna array is proposed in this paper. To the author's best knowledge, this is the first time to use conformal MTS to construct antenna array. The wideband MTS antenna element having 4×4 square unit cells fed by an L-probe is proposed. The initial model was proposed in [31], but no measurement and analysis are given. Moreover, the feeding L-probe is hard to manufacture. Different from other wideband MTS antennas using multi modes [32], [33], only one resonant mode of the proposed antenna element is excited to achieve a broad band. Most works focus on the planar metasurface antenna array, but we use the conformal MTS to construct the antenna array. The conformal antenna array with a bending angle of 10° is constructed by 4×8 MTS antenna elements to exhibit an IMBW of 2.8-3.63 GHz (0.82 GHz, 25.6%) and a peak gain of 20.2 dBi. Our antenna provides a new way to design a compact, low profile, and wideband conformal antenna array, which is desired in many applications, such as airport surveillance radar for air traffic control, weather radar, and some communications satellites.

II. DESIGN AND ANALYSIS OF THE ANTENNA ELEMENT

A. ANTENNA ELEMENT

The configuration of the MTS antenna is presented in Fig. 1, consisting of an MTS, an L-probe, and a square metal ground. A tapered microstrip line is used to feed the MTS antenna. The MTS composed of 4×4 square patches is placed on the rear side of substrate Sub 1 and located at a distance of $H = 8$ mm above the ground. The L-probe, having a short horizontal metal strip printed on the top side of Sub 1 along y-direction and a vertical probe embedded through Sub 1, is connected to the end of the tapered feeding line. The tapered microstrip line is etched on the front side of the lower substrate Sub 2. Four nylon posts in the corners

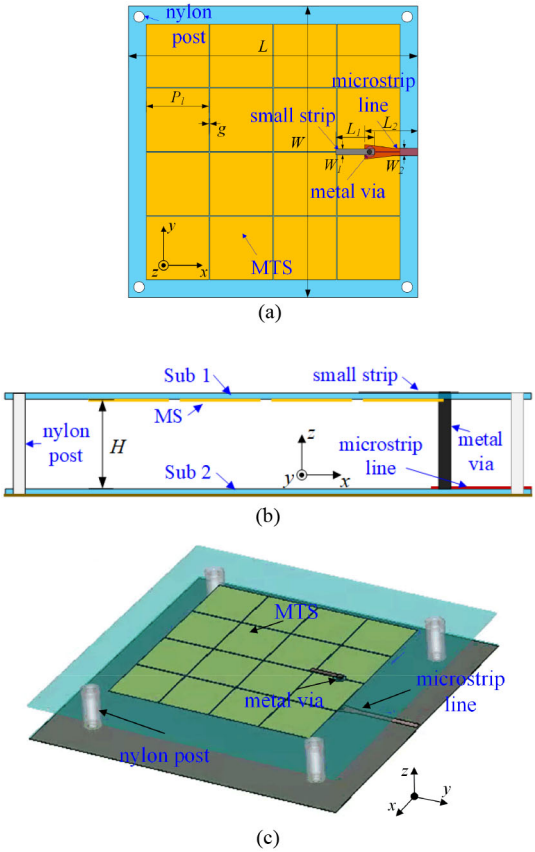

FIGURE 1. Geometry of the antenna element, (a) top view, (b) side view and (c) 3D view.

TABLE 1. Dimensions of proposed antenna element (mm).

Parameters	L	L_1	L_2	W	W_1	W_2	H	P_1	g
Value	60	8	65	60	1.2	1.54	8	13	0.2

are used to keep the air distance between the MTS and the metal ground.

Both the substrates Sub 1 and Sub 2 are made of F4b substrates, with a thickness 0.5 mm and dielectric constant of 2.2. The thin dielectric substrates provide a possibility for the lateral conformal application. The detailed geometric dimensions of the antenna element are displayed in Table 1, with a total size of 60×60×9 mm^3 (0.64×0.64×0.09 λ_0^3, where λ_0 is the free space wavelength at 3.2 GHz).

The simulated reflection coefficient and realized gain of the antenna element is presented in Fig. 2. It can be found that the simulated impedance bandwidth (IMBW) of the element for S11 < −10 dB is from 2.75 to 3.65 GHz (0.9 GHz, 28.1%). The antenna element exhibits a stable gain between 6.1 and 8.35 dBi across 2.75-3.65 GHz at broadside. The current distributions on the MTS at 2.9 and 3.4 GHz are demonstrated in Fig. 3. It can be found the current distributions are similar across the operating band, and the current concentrates along the gaps between the unit cells of the MTS for radiation. The net currents of the dual resonant frequencies are both towards −y-direction. Although

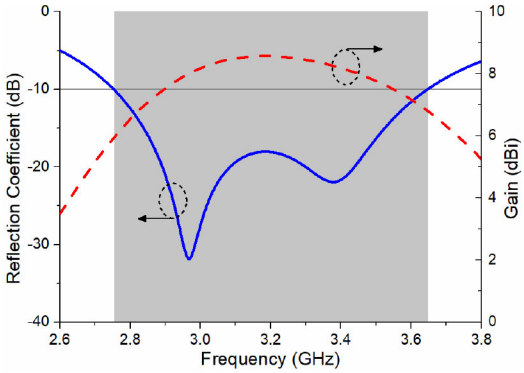

FIGURE 2. Simulated reflection coefficient and gain of the proposed MTS antenna element.

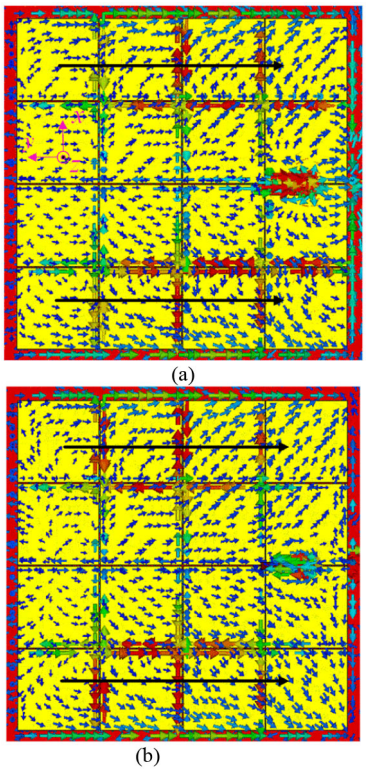

FIGURE 3. Current distributions at (a) 2.9 GHz, (b) 3.4 GHz.

two deep resonances can be observed from Fig. 2, both the resonant frequencies are working in the same mode because of the similar current distributions, which is different from other works using multiple modes [32], [33]. Fig. 4 depicts the simulated normalized radiation patterns at 3.2 GHz in the two principle planes. The radiation patterns keep unidirectional towards $+z$ direction, and the broadside cross polarization discrimination is more than 37 dB. Moreover, the simulated front-back ratio of the radiation pattern is greater than 13 dB.

The L-probe fed patch antenna with the same height as the proposed antenna is also designed to compare the performance. Simulated results show that the bandwidth of the L-probe fed patch antenna is only 10%, which is narrower

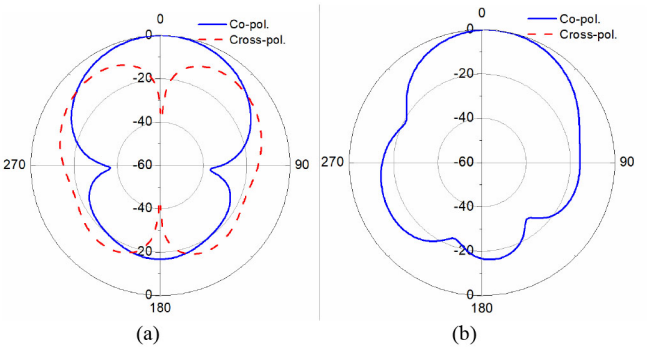

FIGURE 4. Simulated radiation patterns of the element at 3.2 GHz in the (a) *x-z* and (b) *y-z* plane.

than the proposed antenna. Thus, combining the L-probe and the MTS can realize a wide bandwidth.

B. CMA ANALYSIS OF THE METASURFACE

To investigate the operating mechanism of the MTS antenna element, the proposed MTS is studied using the theory of characteristic modes (TCM). In the TCM, the modal behavior can be evaluated based on the generalized eigenvalue equation $\boldsymbol{XJ}n = \lambda n\boldsymbol{RJ}n$, where $\boldsymbol{R}$ and $\boldsymbol{X}$ are the real and imaginary Hermitian parts of the generalized impedance matrix $\boldsymbol{Z} = \boldsymbol{R} + j\boldsymbol{X}$ [32], and $\boldsymbol{J}n$ and λn represent the eigenvector and eigenvalue for mode n. Note that any induced current $\boldsymbol{J}$ on the conductor can be regarded as a linear superposition of normalized characteristic currents $\boldsymbol{J}_n$ as $\boldsymbol{J} = \sum \alpha_n \boldsymbol{J}_n$, where $\boldsymbol{J}$ assembles a complete orthogonal set of modal currents $\boldsymbol{J}_n$, and α_n determines the weighting coefficient of each mode. To analyze the resonant frequency and the potential contribution to the radiation of each mode more conveniently, the modal significance (MS) is expressed as $\mathrm{MS} = |1/(1 + j\lambda n)|$. The MS ranges from 0 to 1, where $\mathrm{MS} = 1$ means that the mode resonates and radiates with the maximal efficiency and $\mathrm{MS} = 0$ means the mode hardly resonates and radiates. When the MS value of a mode is within 0.707∼1, that mode is considered significant, which is suitable for antenna design [34].

An array of 4×4 square patches etched on the top surface of the F4b substrate constructs the MTS. The MS, modal currents and modal radiation patterns of the first four characteristic modes of the MTS without any feeding structure are investigated by the MoM-based CMA tool in commercial simulation software CST MWS, which are depicted in Fig. 5 and Fig. 6. As shown, the MS of Mode 1 is greater than 0.707 within 2.75-3.65 GHz, but the current distribution of Mode 1 forms a loop, resulting a conical radiation pattern which is undesired. Mode 2 and Mode 3 have the same MS, which is higher than 0.707 within the working frequency band. The current distributions of the two modes are along x- and y-axis, respectively. Thus, $\boldsymbol{J_2}$ and $\boldsymbol{J_3}$ are a pair of orthogonal modes, having the orthogonal radiation patterns. Mode 4 has reverse currents along the MTS,

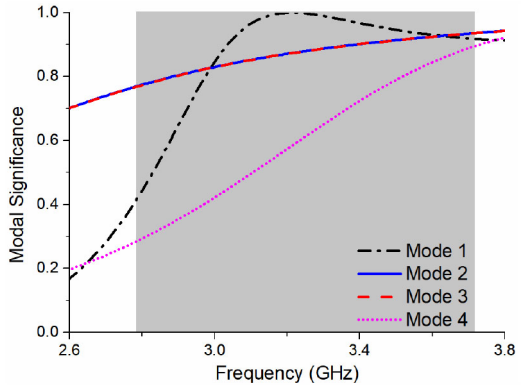

FIGURE 5. Modal significance of the MTS without feeding structure.

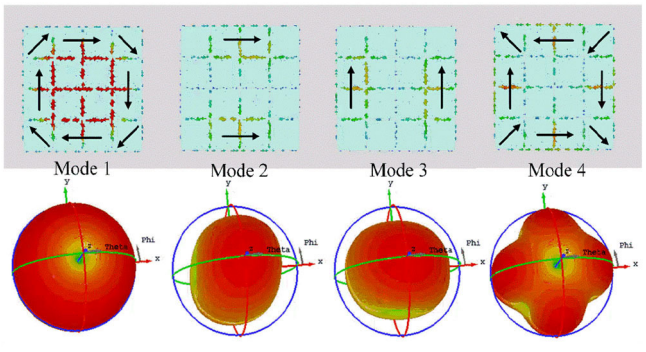

FIGURE 6. Modal currents and radiation patterns of the proposed MTS at 3.2 GHz.

resulting a radiation pattern with a null at broadside direction. Thus, Mode 2 and Mode 3 are the desired modes to generate unidirectional radiation within the operating band. By employing proper feeding technique to excite either of the two modes, the MTS antenna can achieve linearly polarized unidirectional radiation. Compared with Fig. 3, the current distribution of Mode 2 is quite similar to that of MTS antenna with L-probe feeding. The MS of Mode 2 is always higher than 0.707 within 2.75-3.65 GHz, which also proves that the proposed antenna is working in the same mode.

III. CONFORMAL ANTENNA ARRAY AND EXPERIMENTAL RESULTS

A. ANTENNA ARRAY CONFIGURATION

Based on the MTS antenna in Section II, a 4×8 planar antenna array is designed with an overall size of $443\times350\times9$ mm^3 ($4.59\times3.74\times0.09\ \lambda_0^3$). The configuration of the planar antenna array is displayed in Fig. 7. For the conformal application, the fabricated planar array is mounted on the curving surface of a bracket made by 3D printing technique. The degree of bending is determined by different conformal angle θ in Fig. 7(c), corresponding to different radius of the sector.The proposed antenna array is constructed by a simple feeding network and 4×8 antenna elements. The feeding network is composed of a series of T-type power dividers, as shown in Fig. 7(a). The simulated scattering coefficients of the whole feeding network without

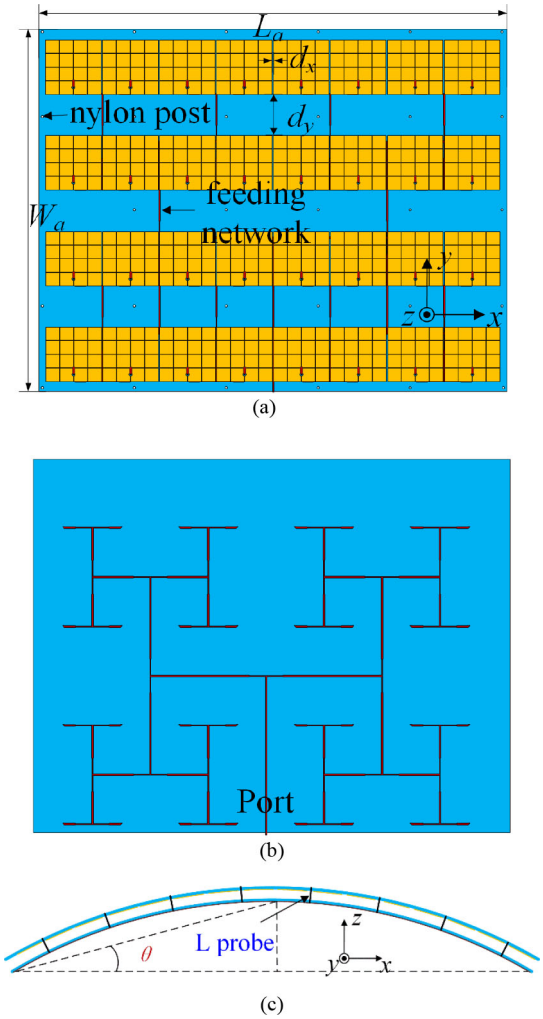

FIGURE 7. (a) Top view, (b) feeding network of the proposed antenna array, and (c) side view of the conformal structure.

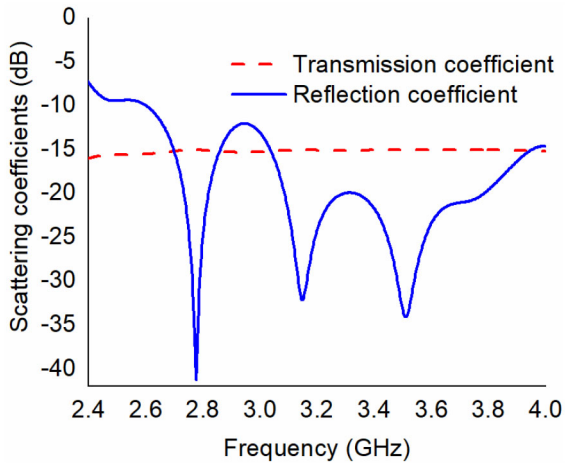

FIGURE 8. Scattering coefficients of the feeding network.

the antenna are shown in Fig. 8, indicating the reflection coefficient is below −10 dB from 2.6 to 4.0 GHz, and the transmission coefficient is around −15 dB.

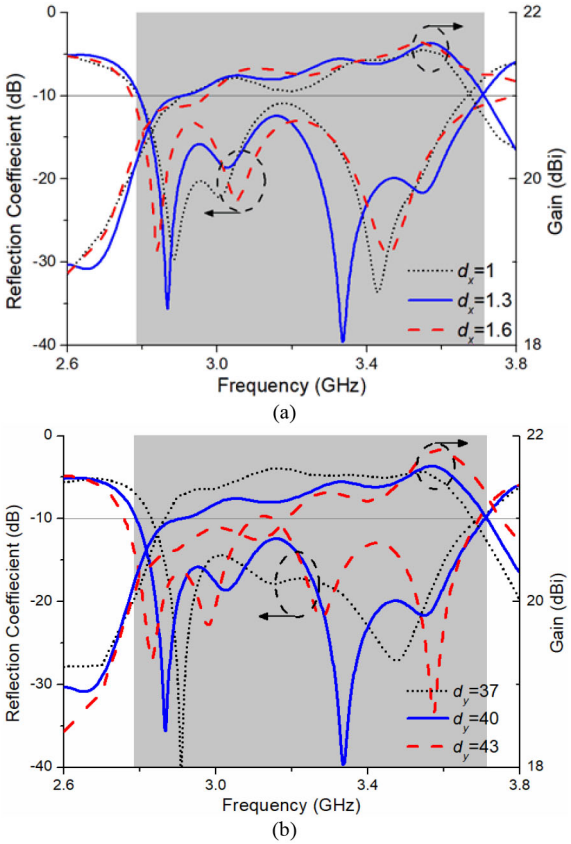

FIGURE 9. Simulated reflection coefficients and gains with different (a) d_X, and (b) d_Y.

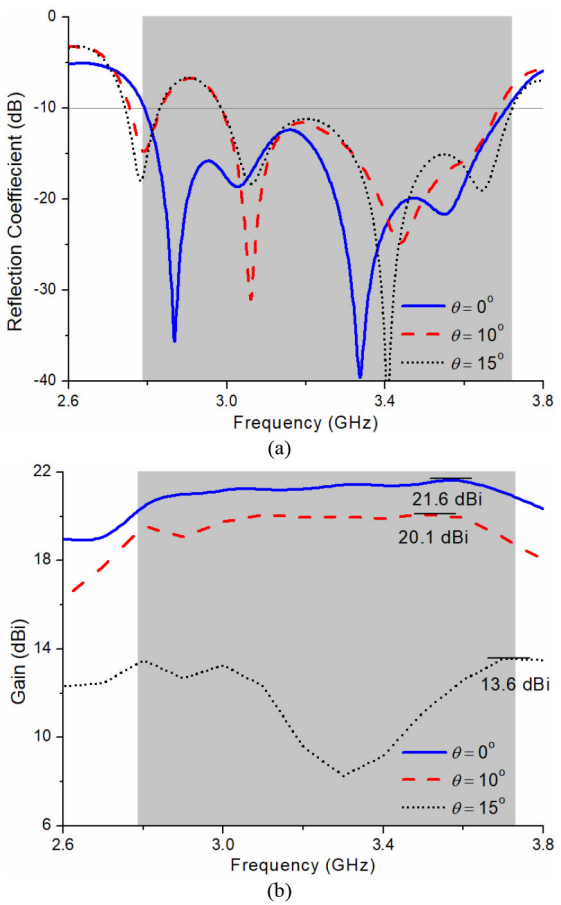

FIGURE 10. (a) Simulated reflection coefficients, (b) broadside gains of the proposed antenna array with different angles.

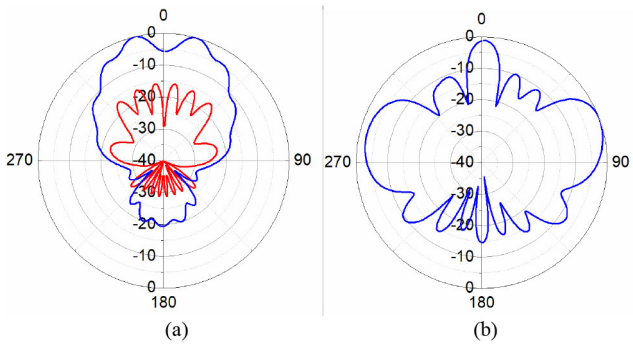

FIGURE 11. Simulated radiation pattern at 3.2 GHz in dBi for $\theta = 15°$ (a) *x-z* plane, and (b) *y-z* plane.

The effects of the distances in the x- and y-directions on the antenna performance are studied in Fig. 9. It can be found that with d_x increases from 1 to 1.3 and 1.6 mm, the bandwidth and gain of the proposed array are similar. When d_y increases from 37 to 40 and 43 mm, the bandwidth of the antenna array increases but the gain decreases. Thus, to achieve a wideband IMBW and balanced high gain performance with a compact size, the distance between the elements are optimized with $d_x = 1.3$ mm and $d_y = 40$ mm. Due to the small distance between the antenna elements along x-direction, an isolation below -12.4 dB is observed between two elements by simulation. Due to the symmetrical antenna array structure and single port feeding, the mutual coupling does not degrade the radiation pattern.

Then, the conformal antenna array are investigated. Two cases of $\theta = 10°$ and $\theta = 15°$ are studied, and the reflection coefficients and broadside gains are given in Fig. 10 for comparison. The simulated IMBW of the planar structure is 2.79-3.71 GHz (0.92 GHz, 28.8%), while the IMBWs of the conformal structures are about the same, but with a poor matching at around 2.9 GHz. Note that the planar structure equals to $\theta = 0°$. With the increase of the bending angles from $\theta = 0°$ to $10°$ and $15°$, the peak gain at broadside becomes lower from 21.6 to 20.1 and 13.6 dBi. The average gain drop between $\theta = 0°$ to $\theta = 10°$ is about 1.5 dB, while the gain of $\theta = 15°$ decreases much larger. By observing the radiation pattern of $\theta = 15°$ in Fig. 11, the peak lobe direction of the radiation pattern in the x-z plane is not towards broadside and a big gain drop is generated. Thus, the proposed conformal antenna array can remains wide band performance and high unidirectional radiation when the conformal angle $\theta \leq 10°$, but has a poor unidirectional radiation performance for $\theta = 15°$.

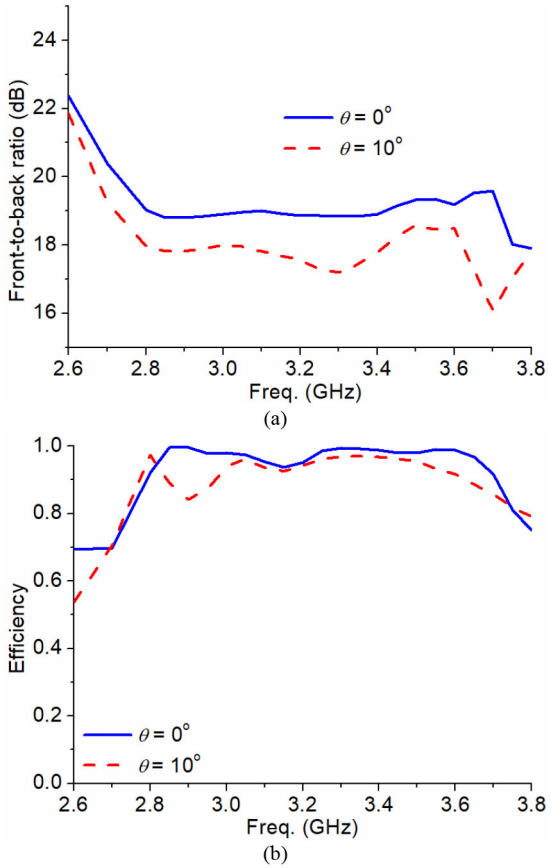

FIGURE 12. (a) Simulated front-to-back ratios and (b) radiation efficiencies of the planar and conformal antenna arrays.

When the bending angle becomes large, the relative phases of the transmitted or received EM wave of each antenna element will vary, leading to the degradation of the radiation pattern.

Since the unidirectional radiation performance can be maintained when the bending angle is smaller than 10°, the simulated front-to-back ratios and radiation efficiencies of the planar and conformal antenna arrays are shown in Fig. 12. Within 2.79-3.71 GHz, the front-to-back ratios are more than 18.7 dB and 16 dB for the planar and conformal antenna arrays, respectively. The simulated efficiencies of the planar and conformal antenna arrays are greater than 91% and 84%, respectively.

Based on the above results, the design procedure is given as follows.

1. Analyze the characteristic modes of the MTS based antenna element to select the working mode for wideband unidirectional radiation, adjust P_1 and g to obtain the required frequency band.

2. Apply the L-probe feeding for linearly polarization, and adjust the dimensions of the L-probe to obtain the required IMBW.

3. Design the feeding network based on the antenna number, and combine the MTS array and the feeding network together.

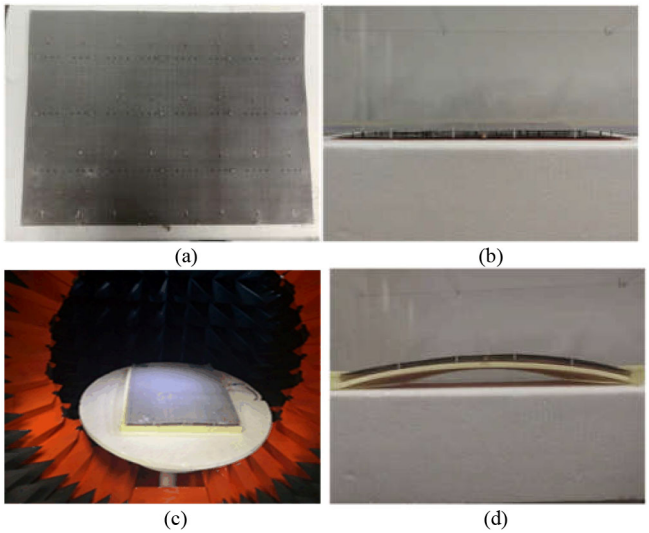

FIGURE 13. (a) Top and (b) side views of the planar antenna array, (c) top and (d) side views of the conformal antenna array.

4. Bend the antenna array to see the radiation pattern and IMBW, and find the biggest bending angle to maintain the unidirectional radiation performance.

B. SIMULATED AND MEASURED RESULTS

The antenna array was simulated, fabricated and measured to verify the design. The manufacture model of the antenna array is shown in Fig. 13. The simulated and measured reflection coefficients of the planar antenna array are depicted in Fig. 14. It is seen that the simulated and measured IMBWs of the planar structure are 2.79-3.71 GHz (0.92 GHz, 28.8%) and 2.81-3.76 GHz (0.95 GHz, 29.7%), respectively. For comparison, the simulated and measured reflection coefficients of the conformal antenna array with $\theta = 10°$ and $\theta = 15°$ are also shown in Fig. 14(b). The measured results show that the conformal antenna still remains a wide band of 2.8-3.63 GHz (0.82 GHz, 25.6%). The difference of the simulated and measured results could be due to the fabrication and measurement tolerances. The conformal bracket made by 3D printing technique may also have fabrication error, which affects the measured results.

The simulated and measured broadside gains of the planar and conformal array are presented in Fig. 14(c). The simulated broadside gain of the planar structure varies from 20.4 dBi to 21.6 dBi with a gain variation of 1.2 dB within the working band, and the measured broadside gain varies from 18.5 dBi to 22.2 dBi. The simulated and measured realized gains with conformal angle $\theta = 10°$ ranges from 19.0 to 20.1 dBi and 17.2 to 20.2 dBi, respectively. The reduction of the broadside gains can be owing to the increase of the radiation side lobes caused by bending deformation.

The simulated and measured normalized radiation patterns of the planar and conformal antenna array at the center

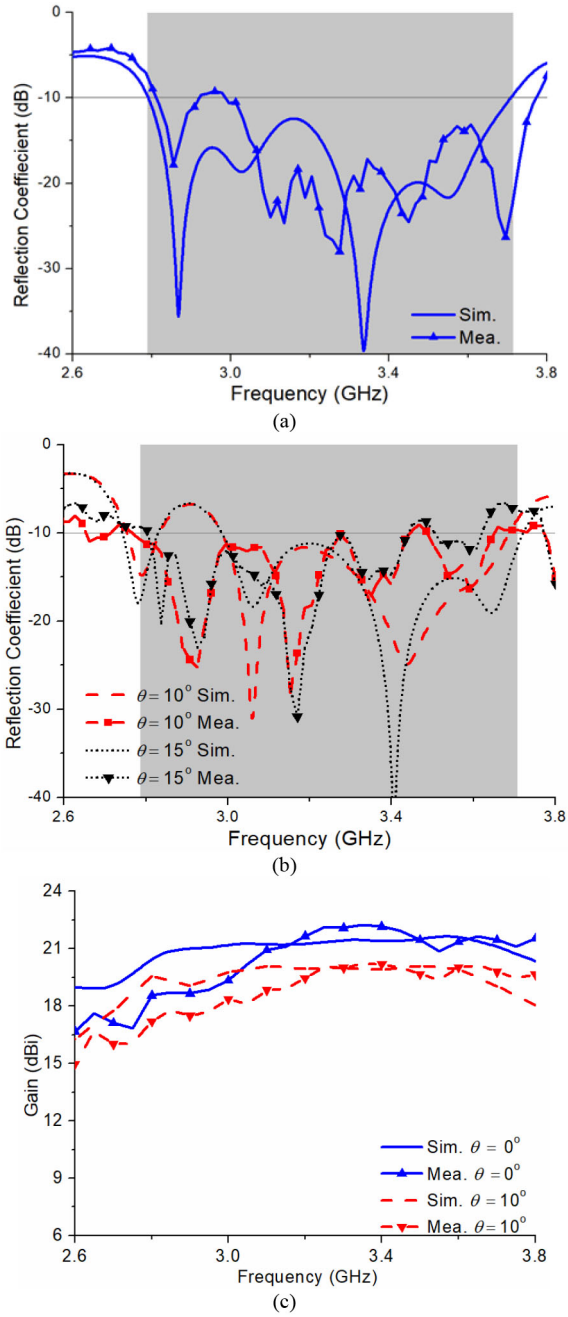

FIGURE 14. Simulated and measured reflection coefficients (a) θ = 0° (planar structure), (b) θ = 10° and θ = 15° (conformal structure), (c) realized broadside gains of the antenna array.

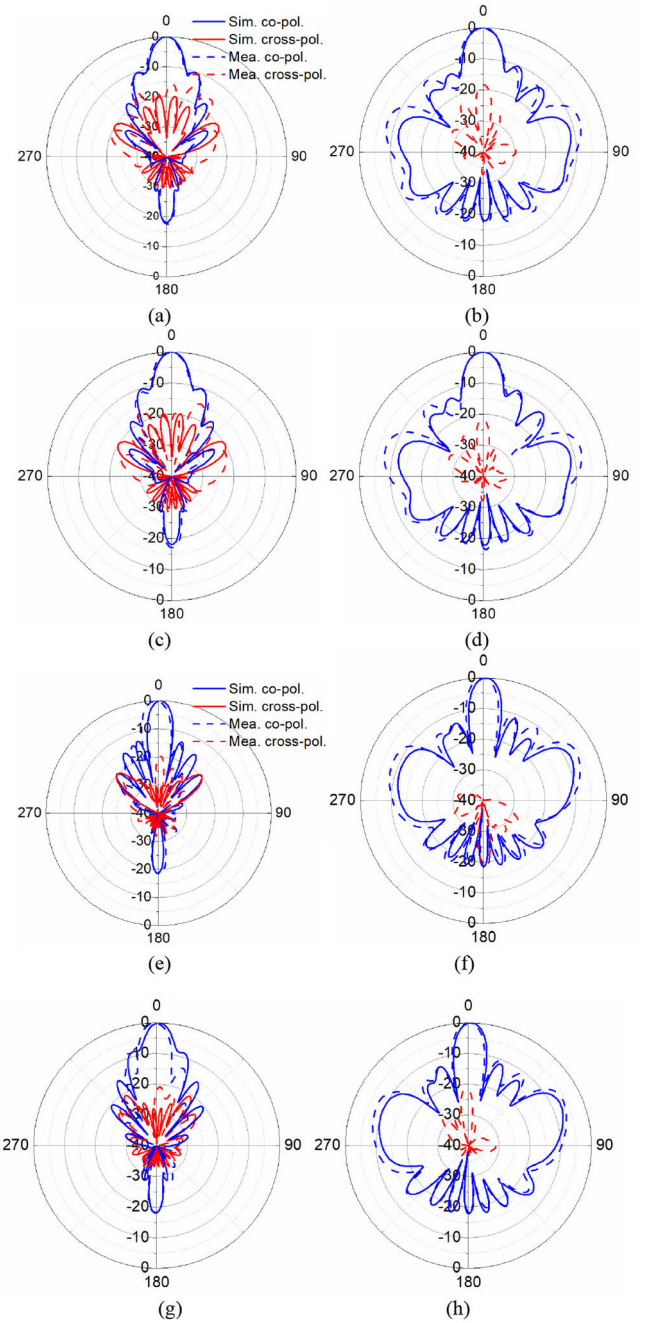

FIGURE 15. Simulated and measured radiation patterns at 2.8 GHz in dBi. (a) *x-z* plane and (b) *y-z* plane with $\theta = 0°$, (c) *x-z* plane and (d) *y-z* plane with $\theta = 10°$, at 3.2 GHz in dBi (e) *x-z* plane and (f) *y-z* plane with $\theta = 0°$, (g) *x-z* plane and (h) *y-z* plane with $\theta = 10°$.

frequency of 3.2 GHz are shown in Fig. 15. The radiations patterns of the planar array are unidirectional across the operating band, and have a cross-polarization discrimination lower than −20 dB in both *E*- and *H*-planes in the broadside direction. The planar antenna array has a 3-dB beamwidths of 10.7° and 12.4° in the *x-z* and *y-z* planes in simulation, and the measured 3-dB beamwidths are 11.9° and 13.2°. For the conformal antenna with $\theta = 10°$, the cross polarization discrimination is lower than −22 dB at broadside. The simulated 3-dB beamwidths are 10.9° and 12.4° in the *x-z* and *y-z* planes, and the measured 3-dB beamwidths are 12.2° and 12.6°. The simulated and measured front-to-back ratio of the radiation patterns are both about 19 dB.

Finally, the performance of the proposed conformal MTS antenna is compared with other conformal works using MTS in Table 2. In can be observed that the proposed antenna exhibits the widest bandwidth, and the gain is higher than others except [28].

TABLE 2. Comparison with other conformal MTS-based antennas.

Ref	Center Freq. (GHz)	Cross section size (mm^2)	Height (mm)	Bending angle (θ)	Bandwidth	Peak gain (dBi)	Radiation pattern
26	10	100×5 ($33.3\times0.16\ \lambda_0^2$)	100 ($33.3\lambda_0$)	45°	2%	5	Omni-directional
27	5.7	60×330 ($1.14\times6.27\ \lambda_0^2$)	NG	NG	1.7%	10.3	Uni-directional
28	10	75.7×93.5 ($2.52\times3.11\ \lambda_0^2$)	51.5 ($1.71\lambda_0$)	23.6°	8%	20.6	Uni-directional
29	10	90×300 ($3\times10\ \lambda_0^2$)	150 ($5\lambda_0$)	45°	1%	18.6	Uni-directional
30	5.75	400×212.5 ($7.67\times4.07\ \lambda_0^2$)	200 ($3.83\lambda_0$)	45°	5%	14.3	Uni-directional
Pro	3.2	434×350 ($4.62\times3.73\ \lambda_0^2$)	47.2 ($0.5\lambda_0$)	10°	25.6%	20.2	Uni-directional

IV. CONCLUSION

In this paper, a broadband conformal MTS antenna array with high gain fed by L-probes is proposed for curving platform application. The combination of the periodic MTS structure and L-probe feeding result a low profile and broad bandwidth. The proposed MTS element is investigated with the TCM and achieves a wide IMBW with a single mode. The proposed antenna array is composed of a simple feeding network and 4×8 antenna elements. Simulated and measured results indicate that the planar antenna array has the IMBWs of 2.79-3.71 GHz (0.92 GHz, 28.3%) and unidirectional radiation patterns with balanced high gains of 21±0.6 dBi within the operating band. Finally, the conformal array is investigated by two conformal angle cases of $\theta = 10°$ and $\theta = 15°$, and the unidirectional radiation patterns can be retained for $\theta \leq 10°$. Therefore, the proposed MTS antenna exhibits the merits of low profile, wideband and high gain, and is a good candidate of aircrafts, UAVs, and automobiles applications.

REFERENCES

[1] N. Yu *et al.*, "Light propagation with phase discontinuities: Generalized laws of reflection and refraction," *Science*, vol. 334, no. 6054, pp. 333–337, 2011.

[2] H. F. Ma, G. Z. Wang, G. S. Kong, and T. Cui, "Independent controls of differently-polarized reflected waves by anisotropic metasurfaces," *Sci. Rep.*, vol. 5, p. 9605, Apr. 2015.

[3] W.-L. Guo, G.-M. Wang, H.-S. Hou, K. Chen, and Y. Feng, "Multi-functional coding metasurface for dual-band independent electromagnetic wave control," *Opt. Exp.*, vol. 27, no. 14, pp. 19196–19211, 2019.

[4] X. M. Ding *et al.*, "Ultrathin Pancharatnam–Berry metasurface with maximal cross-polarization efficiency," *Adv. Mater.*, vol. 27, no. 7, pp. 1195–1200, 2015.

[5] S. Sun *et al.*, "High-efficiency broadband anomalous reflection by gradient meta-surfaces," *Nano Lett.*, vol. 12, no. 12, pp. 6223–6229, 2012.

[6] X. Liu *et al.*, "Perfect anomalous reflection and refraction utilizing binary Pancharatnam–Berry phase elements based metasurfaces," *J. Phys. D, Appl. Phys.*, vol. 53, no. 6, 2020, Art. no. 065111.

[7] H. L. Zhu, S. W. Cheung, X. H. Liu, and T. I. Yuk, "Design of polarization reconfigurable antenna using metasurface," *IEEE Trans. Antennas Propag.*, vol. 62, no. 6, pp. 2891–2898, Jun. 2014.

[8] J. M. Zhang *et al.*, "High-efficiency polarization conversion phase gradient metasurface for wideband anomalous reflection," *J. Appl. Phys.*, vol. 122, no. 1, Art. no. 014501, 2017.

[9] Q. Lv, C. Jin, B. Zhang, and Z. Shen, "Hybrid absorptive-diffusive frequency selective radome," *IEEE Trans. Antennas Propag.*, vol. 69, no. 6, pp. 3312–3321, Jun. 2020.

[10] Y. Liu, K. Li, Y. Jia, Y. Hao, S. Gong, and Y. J. Guo, "Wideband RCS reduction of a slot array antenna using polarization conversion metasurfaces," *IEEE Trans. Antennas Propag.*, vol. 64, no. 1, pp. 326–331, Jan. 2016.

[11] W. E. I. Liu, Z. N. Chen, and X. Qing, "Broadband low-profile L-probe fed metasurface antenna with TM leaky wave and TE surface wave resonances," *IEEE Trans. Antennas Propag.*, vol. 68, no. 3, pp. 1348–1355, Mar. 2020.

[12] C. Zhou, S. W. Cheung, Q. Li, and M. Li, "Bandwidth and gain improvement of a crossed slot antenna with metasurface," *Appl. Phys. Lett.*, vol. 110, no. 21, pp. 1–5, 2017.

[13] W. Liu, Z. N. Chen, and X. M. Qing, "Metamaterial-based low-profile broadband mushroom antenna," *IEEE Trans. Antennas Propag.*, vol. 62, no. 3, pp. 1165–1172, Mar. 2014.

[14] G. Liu, X. Sun, X. Chen, D. Xiong, M. Li, and M.-C. Tang, "A broadband low-profile dual-linearly polarized dipole-driven metasurface antenna," *IEEE Antennas Wireless Propag. Lett.*, vol. 19, no. 10, pp. 1759–1763, Oct. 2020.

[15] C. F. Zhou and S. W. Cheung, "Metasurface-based antenna excited by the slotted radiator," *J. Electromagn. Waves Appl.*, vol. 32, no. 16, pp. 2086–2098, 2018.

[16] N.-S. Nie, X.-S. Yang, Z. N. Chen, and B. Z. Wang, "A low-profile wideband hybrid metasurface antenna array for 5G and WiFi systems," *IEEE Trans. Antennas Propag.*, vol. 68, no. 2, pp. 665–671, Feb. 2020.

[17] B. S. Abirami, E. F. Sundarsingh, and A. Harshavardhini, "A compact conformal windshield antenna for location tracking on vehicular platforms," *IEEE Trans. Vehicular Tech.*, vol. 68, no. 4, pp. 4047–4050, Apr. 2019.

[18] S. Ogurtsov and S. Koziel, "A conformal circularly polarized series-fed microstrip antenna array design," *IEEE Trans. Antennas Propag.*, vol. 68, no. 2, pp. 873–881, Feb. 2020.

[19] B. Mohamadzade, R. B. V. B. Simorangkir, R. M. Hashmi, Y. C.-Oger, M. Zhadobov, and R. Sauleau, "A conformal band-notched ultrawideband antenna with monopole-like radiation characteristics," *IEEE Antennas Wireless Propag. Lett.*, vol. 19, no. 1, pp. 203–207, Jan. 2020.

[20] M. Boyuan, J. Pan, E. Wang, and Y. Luo, "Conformal bent dielectric resonator antennas with curving ground plane," *IEEE Trans. Antennas Propag.*, vol. 67, no. 3, pp. 1931–1936, Mar. 2019.

[21] B. Mohamadzade, R. B. V. B. Simorangkir, R. M. Hashmi, and A. Lalbakhsh, "A conformal ultrawideband antenna with monopole-like radiation patterns," *IEEE Trans. Antennas Propag.*, vol. 68, no. 8, pp. 6383–6388, Aug. 2020.

[22] X. Gao, Z. Shen, and C. Hua, "Conformal VHF log-periodic balloon antenna," *IEEE Trans. Antennas Propag.*, vol. 63, no. 6, pp. 2756–2761, Jun. 2015.
[23] Y. Wang, J. Su, Z. Li, Q. Guo, and J. Song, "A prismatic conformal metasurface for radar cross-sectional reduction," *IEEE Antennas Wireless Propag. Lett.*, vol. 19, no. 4, pp. 631–635, Apr. 2020.
[24] Y. Wang, F. Qi, Z. Liu, P. Liu, and W. Li, "Ultrathin and flexible reflective polarization converter based on metasurfaces with overlapped arrays," *IEEE Antennas Wireless Propag. Lett.*, vol. 19, no. 12, pp. 2512–2516, Dec. 2020.
[25] C. Fu, L. Han, C. Liu, X. Lu, and Z. Sun, "Combining Pancharatnam-Berry phase and conformal coding metasurface for dual-band RCS reduction," *IEEE Trans. Antennas Propag.*, early access, Sep. 20, 2021, doi: 10.1109/TAP.2021.3112618.
[26] K.-Y. Liu, G.-M. Wang, T. Cai, H.-P. Li, and T.-Y. Li, "Conformal polarization conversion metasurface for omni-directional circular polarization antenna application," *IEEE Trans. Antennas Propag.*, vol. 69, no. 6, pp. 3349–3358, Jun. 2021.
[27] D. Germain, D. Seetharamdoo, S. N. Burokur, and A. De Lustrac, "Phase-compensated metasurface for a conformal microwave antenna," *Appl. Phys. Lett.*, vol. 103, no. 12, 2013, Art. no. 124102.
[28] L.-Z. Song, P.-Y. Qin, and Y. J. Guo, "A high-efficiency conformal transmitarray antenna employing dual-layer ultrathin huygens element," *IEEE Trans. Antennas Propag.*, vol. 69, no. 2, pp. 848–858, Feb. 2021.
[29] Y. Shang, W. Zhou, and C. Liao, "Metasurface-based cylindrical lenses and their antenna gain enhancement," *Int. J. Antennas Propag.*, vol. 2020, Sep. 2020, Art. no. 7393658.
[30] H. Li *et al.*, "Wide-angle beam steering based on an active conformal metasurface lens," *IEEE Access*, vol. 7, pp. 185264–185272, 2019.
[31] S. Yuan, C. Zhou, and H. Li, "A wideband L-probe fed antenna based on metasurface with high efficiency," in *IEEE 3rd Int. Conf. Electron. Inf. Commun. Technol. (ICEICT)*, Shenzhen, China, 2020, pp. 1–3.
[32] F. H. Lin and Z. N. Chen, "Low-profile wideband metasurface antennas using characteristic mode analysis," *IEEE Trans. Antennas Propag.*, vol. 65, no. 4, pp. 1706–1713, Apr. 2017.
[33] W. E. I. Liu, Z. N. Chen, X. Qing, J. Shi, and F. H. Lin, "Miniaturized wideband metasurface antennas," *IEEE Trans. Antennas Propag.*, vol. 65, no. 12, pp. 7345–7349, Dec. 2017.
[34] Q. Li and T.-Y. Shih, "Characteristic-mode-based design of planar in-band full-duplex antennas," *IEEE Open J. Antennas Propag.*, vol. 1, pp. 329–338, 2020.